Gyrokinetic analysis of inter-ELM transport mechanisms in a DIII-D pedestal

M.R. Halfmoon, D.R. Hatch, M.T. Kotschenreuther, S.M. Mahajan, and M. Curie
Institute for Fusion Studies, University of Texas at Austin, Austin, TX

A.O. Nelson, E. Kolemen, and A. Diallo
Princeton Plasma Physics Lab, Princeton University, Princeton, NJ

R.J. Groebner, E.A. Belli, and J. Candy
General Atomics, San Diego, CA

E. Hassan
Oak Ridge National Laboratory, Oak Ridge, TN and
Physics, Faculty of Science, Ain Shams University, Cairo 11566, EG
(Dated: April 9, 2022)

In this study, gyrokinetic simulations are used to study pedestal fluctuations for DIII-D discharge 174082 using the GENE code. Nonlinear local simulations indicate that electron heat flux has contributions from electron temperature gradient (ETG)-driven transport, but at levels insufficient to satisfy power balance. We show that Microtearing modes (MTM) and neoclassical transport are likely to account for the remaining observed energy losses in the electron and ion channels, respectively. The MTM instabilities found in the simulations are consistent with the high frequency fluctuations identified in the magnetic fluctuation data from Mirnov coils. The fluctuation data in this discharge also exhibits a low frequency band of fluctuations. By modifying the equilibrium profiles and plasma β, simulations produce MHD modes, which may be responsible for these observed low frequency fluctuations.

I. INTRODUCTION

The Edge Transport Barrier (ETB), or pedestal, is a thin region in an H-mode plasma that is characterized by inhibited transport[1] due to the suppression of the deleterious combination of ion temperature gradient (ITG) and trapped electron mode (TEM) instabilities. The formation of a pedestal with sufficiently high temperature will be a requirement for the success of ITER.

Several modes have emerged as viable candidates for the mechanism behind observed anomalous density and energy transport in pedestals. These instabilities include: electron temperature gradient (ETG) modes, kinetic ballooning modes (KBMs), and microtearing modes (MTMs), along with the possibility of residual ITG/TEM fluctuations. Gyrokinetic simulations predict that the transport from these micro-instabilities along with neoclassical transport can often be combined to account for observed transport levels within experimental uncertainties.[2–7]

Several studies have examined magnetic fluctuations in the pedestal region via external Mirnov coils[8,9]. Recently, studies have indicated that the MTM is the source of prominent magnetic fluctuations observed in magnetic spectrograms[5,10–13] and a major source of inter-ELM electron heat transport in the steep gradient region of the pedestal[2,13–20]. Figure 1 is a magnetic spectrogram of DIII-D shot 174082, with strong fluctuations at the $\approx 100kHz$ and $\approx 400kHz$ regions (circled in green) and low-frequency ($\approx 50kHz$) magnetic "chatter" (circled in black).

Recent advances in experimental diagnostics on DIII-D have provided internal magnetic fluctuation data via a radial interferometer-polarimeter[10,11]. This technique provides line-integrated calculations of magnetic fluctuations across a chord of the plasma, instead of the traditional technique via external pickup coils. This tool allows for a more direct comparison to gyrokinetic simulations. An initial comparison along these lines will be reported in Ref.[15]

Given this evidence in favor of MTM as a major pedestal transport mechanism, an outstanding question is the role played by the KBM, which is proposed by the EPED model as the salient inter-ELM transport mechanism limiting the pedestal pressure profile[21]. In this paper we consider both MTM and MHD-like modes (such as KBM) as contributors to pedestal transport and the observed magnetic fluctuations.

To this end, we analyze DIII-D shot 174082. In DIII-D discharge 174082 magnetic fluctuation diagnostics produce data that can be clearly identified as MTMs. Specifically, the measured signals between ∼120 kHz and ∼420 kHz in shot 174082 are well within predicted values for MTMs with the equilibrium profiles under consideration, estimating the electron diamagnetic frequency using the

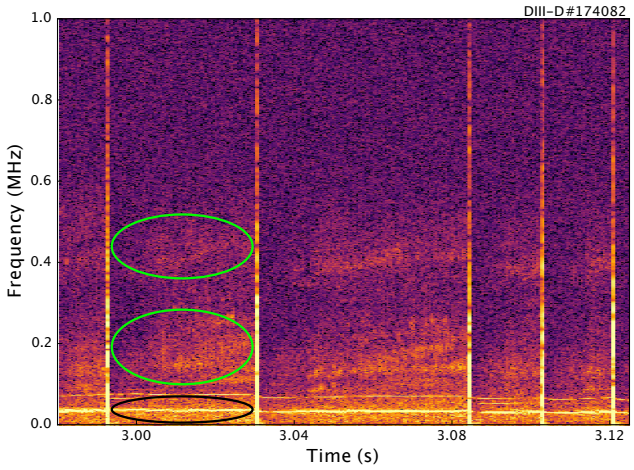

FIG. 1. Fast magnetics of shot 174082. Fluctuations at 0.1 MHz and 0.4 MHz (circled in green) are found across each inter-ELM period. There is also a very low frequency region of activity $< 0.05MHz$ (circled in black).

formula $\omega_{e*} = k_y \rho_s c_s (1/L_{T_e} + 1/L_n)$, where the electron temperature and density gradient scale lengths are L_{T_e,n_e} respectively, ρ_s is the ion gyroradius, c_s the plasma sound speed, and k_y is the binormal wavenumber. We demonstrate this correspondence directly with simulations using the gyrokinetic code GENE[22,23] The experimentally observed frequencies match closely the values identified in our gyrokinetic simulations of MTMs, with global simulations indicating that the MTM is the fastest growing mode.

Given this evidence in favor of MTM, we are also interested in the potential role of MHD-like modes, such as KBMs, which are proposed as a pedestal constraint in the EPED model[21]. Consequently, we carry out several numerical and thought experiments to probe the possible role of MHD modes. By modifying the equilibrium beta, simulations show that the an MHD instability can become the fastest growing global linear mode. These simulations exhibit significantly higher quasilinear (i.e., normalized to other quantities derived from the linear eigenmode) particle fluxes than MTM's and have ion-diamagnetic directed frequencies. They also have frequencies in the range of the low-frequency activity observed in magnetic spectrograms for this discharge.

The paper is outlined as follows: First, the details of the experimental configuration under investigation will be discussed in Sec. II, with emphasis on the methodology of reconstructing profile data. Second, the gyrokinetic simulations performed using these experimental profiles will be laid out in detail III, including the results of: local linear scans in collisionality and perpendicular length scale, global linear scans of length scale, and local nonlinear simulations at the peak in ω_e^*. Third, simulation results will be compared to experimental transport and fluctuation measurements in Sec. IV.

II. EXPERIMENTAL PROFILES AND EQUILIBRIUM

The simulation of anomalous transport in pedestals requires profiles of temperature and density for all relevant particle species, the radial electric field, and a kinetic reconstruction of the magnetic equilibrium. To ensure that all of these effects are accurately obtained from the experimental discharge, extensive work has been performed using experimental diagnostics and modules found in the software suite OMFIT 24. Kinetic equilibria were calculated manually from inter-ELM averaged profiles and compared to results from the CAKE code, which provides self-consistent kinetic equilibria from automatic profile fitting and the EFIT Grad-Shafranov solver[24,25]. All profiles used in this study were then mapped onto the resulting kinetic equilibria. This study focuses on the baseline (174082) equilibrium from a study on the effects of pellet fueling on a neutral beam-heated plasma 25. This shot is heated entirely by neutral beams at a rate of 4.67 MW, with no pellet injection involved. The resulting magnetic geometry and plasma profiles give snapshots of the DIII-D experiment.

This work utilizes the resulting magnetic geometry and profile data as input for the gyrokinetic solver GENE to simulate the inter-ELM onset of pedestal micro-instabilities. To account for the stiffness of the transport mechanisms, sensitivity tests are performed with changes to local equilibrium gradients that fall within the tolerance of these reconstructions. Overall, these equilibria are accurate representations of the inter-ELM steady state for a given shot due to systematic reconstruction via OMFIT, and thus the resulting gyrokinetic simulations are performed with experimental inputs that are as accurate and comprehensive as possible.

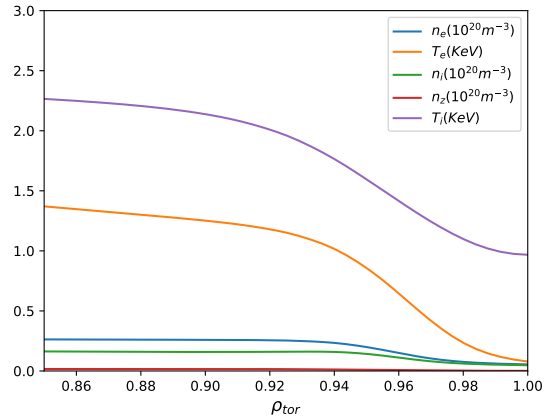

FIG. 2. Density and temperature profiles of the pedestal in baseline shot 174082. Global simulations extend from ρ_{tor} of 0.945 to 0.995.

Figure 2 depicts the density and temperature profiles across the pedestal region. Ion temperature is calculated

using charge exchange recombination (CER), and carbon is treated as an impurity species in simulations. We are also provided $E \times B$ velocity profiles for this shot, allowing for the implementation of shear suppression of other instabilities in these simulations. This $E \times B$ velocity profile is found in Figure 3. The magnetic geometry, pressure profile, q-profile, and P' and FF' source profiles of this shot are shown in Figure 4.

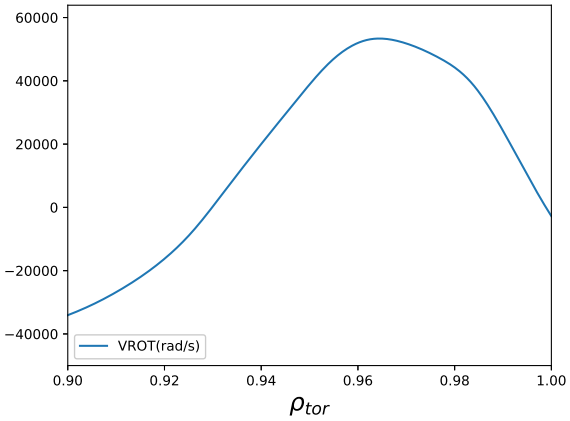

FIG. 3. Plot of the $E \times B$ rotational velocity across the pedestal.

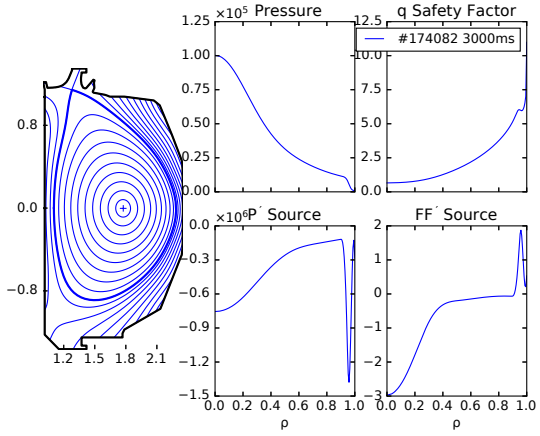

FIG. 4. EFIT profiles of DIII-D shot 174082. Note the local minimum of the q-profile in the pedestal region, previous studies have found a link between low values of magnetic shear, $s = \frac{r}{q}\frac{dq}{dr}$, and a drive to the microtearing mode[14,38].

III. NUMERICAL INVESTIGATIONS

Advances in the gyrokinetic codes have enabled accurate simulations of turbulence in fusion plasmas, matching experimental fluxes to an unprecedented degree. This is particularly true in the core plasma, where gyrokinetic orderings are more strictly satisfied and conditions are less extreme[26–35]. Recently, simulations in the pedestal are also demonstrating increasing correspondence with experimental observations.[2,3,5,6,20,36,37]

The focus of this study is in the region of strongest electron temperature gradient near the plasma edge ($\rho = 0.93 - 0.99$) in order to identify the mechanisms that mediate pedestal development during the inter-ELM cycle and, thus, contribute to the ultimate pre-ELM pedestal structure.

A. Linear Simulations

To gain insight into the driving mechanisms of observed turbulent fluctuations, a series of simulations using the gyrokinetic code GENE[22,23] was run based on the experimental scenario described above, scanning across a wide range of toroidal mode numbers. We consider both local and global simulations. Local linear simulations are performed at $\rho_{tor} = 0.96$ where ω_* peaks. For typical local simulations, a resolution of $(k_x, z, v_\parallel, \mu)$ = (12,96,48,24) is used, while global calculations require $(\rho_{tor}, z, v_\parallel, \mu)$ = (128,96,32,16). Global simulations made use of the block structured grids feature in GENE[39,40], allowing for lower resolutions in velocity space by resizing the velocity space domain to match the background temperature.

Global simulations of the pedestal capture the the radial variation of the background profile, which has been shown to be crucial to understanding the stability of low-n MTM[5,41,42]. In those references, the alignment of mode-rational surfaces with the peak of the ω_{*e} profile was shown to be crucial for low-n MTM instability. In the present scenario, this phenomenon does not appear to be decisive. The critical n number for this sensitive mode-number selection is defined in Ref. [42],

$$n_{crit} = \frac{\rho_{tor}}{2\hat{s}q\mu_{crit}}, \tag{1}$$

where n_{crit} is the critical toroidal mode number, ρ_{tor} is the normalized radial flux surface coordinate, q is the safety factor $d\phi/d\psi$, $\hat{s}$ is the local magnetic shear $(1/q)(dq/dr)$, and μ_{crit} is the distance in ρ between the nearest rational surface and peak in ω_{*e}. For toroidal mode numbers that exceed n_{crit}, multiple rational surfaces are found within the $\delta\rho = 2\mu_{crit}$ range, and the modes are not subject to an offset stabilization effect[42]. The value of n_{crit} for this discharge is ≈ 4. Therefore at toroidal mode number above $n = 4$, instabilities are not suppressed by misalignment between rational surfaces and the ω_* profiles.

Growth rates and frequencies are shown in Fig.5 for both local and global linear simulations. As can be seen, there are multiple branches (peaks). We first demonstrate that the modes are MTMs and subsequently probe the distinction between the branches.

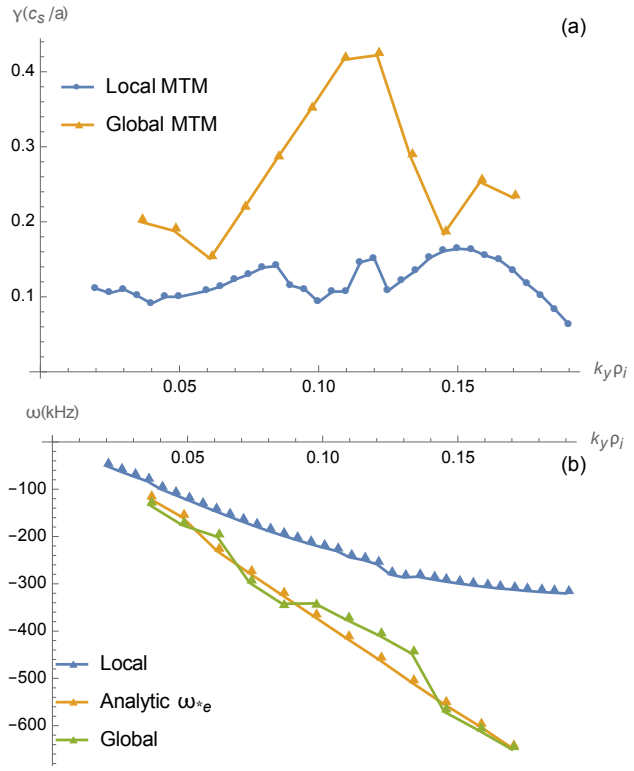

FIG. 5. Growth rates (a) are normalized to ion sound speed over characteristic length scale (c_s/a) as a function of toroidal wavenumber ($k_y\rho_i$) for local (blue) and global (gold) simulations. Local simulations are performed at the $\rho = 0.96$ radial flux surface, with profile input taken directly from experimental equilibrium reconstructions. Real frequencies (b) for local (blue), global (green), and the maximum value of the ω_{*e} profile (gold) in kHz. Discrepancies between local and global frequencies occur as a result of the radial extent of global simulations.

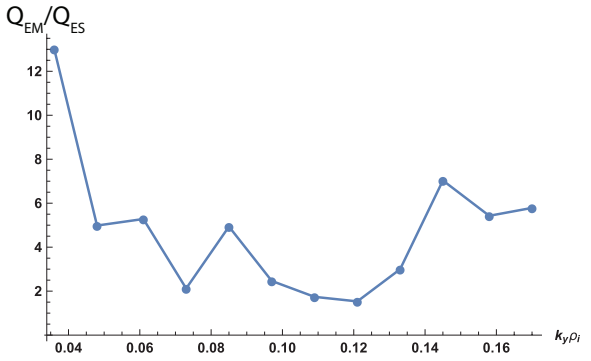

FIG. 6. Plot of the ratio of electromagnetic to electrostatic electron heat flux for a series of global GENE simulations of shot 174082. For MTM's, this ratio is expected to be > 1.

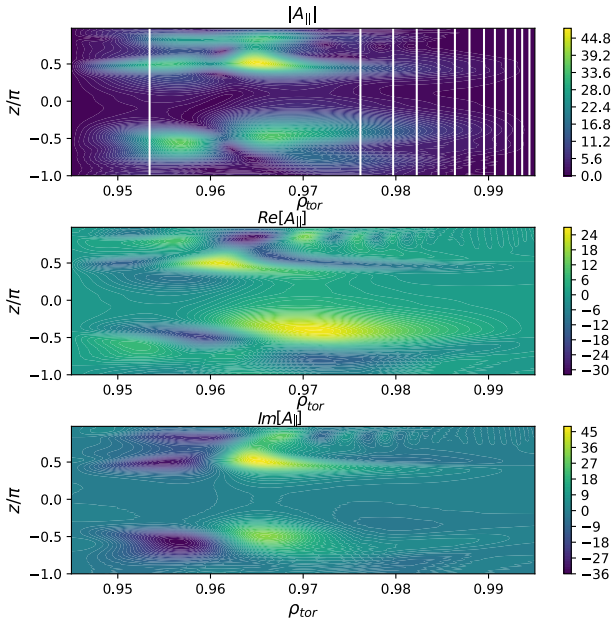

FIG. 7. Example contour of electromagnetic potential for a global linear GENE simulation (n=10). Amplitudes are arbitrary as the simulation is linear. Mode structure displays tearing parity as $A_\parallel$ is an even function.

To establish these modes as MTM, we first note that the experimental frequencies ($\approx 100 - 400kHz$) roughly match the MTM expectation for the given profiles: $\omega = \omega_{*e} = k_y\rho_s c_s \left(\frac{1}{L_{Te}} + \frac{1}{L_n}\right)$, which results in frequencies in the range of $\omega_{*e} = 120 - 500kHz$ for toroidal mode numbers between $n = 3 - 14$ (we will describe detailed comparisons between GENE simulations and the spectrogram below).

Figure 6 depicts for the global linear simulations the ratio Q_{EM}/Q_{ES}, for which a high value is a hallmark of the MTM. An additional point in favor of the MTM is the tearing parity of the $A_{||}$ eigenfuction shown in Fig. 7. Both the real and imaginary parts are roughly symmetric about $z = 0$, indicating even parity for the electromagnetic potential.

Finally, the transport ratios shown in Figure 8 indicate that the electron channel dominates the observed heat flux ($\chi_i/\chi_e << 1$), and the particle flux for each species is small in comparison to the electron heat diffusivity ($D_s/\chi_e << 1$). Although this is also a signature of ETG modes, they can be excluded on the basis of the strong electromagnetic component of the flux and the large scales at which these modes are unstable.

B. Two MTM Branches

Ref. [13] demonstrates that two branches of MTM coexist in the DIII-D pedestal: a slab-like MTM at low n and a curvature-driven mode at higher n. As we show here, we identify the same phenomenon in this discharge, suggesting that it may be quite common in the pedestal. In contrast with Ref. [13], the curvature driven branch in this discharge is unstable at lower toroidal mode numbers

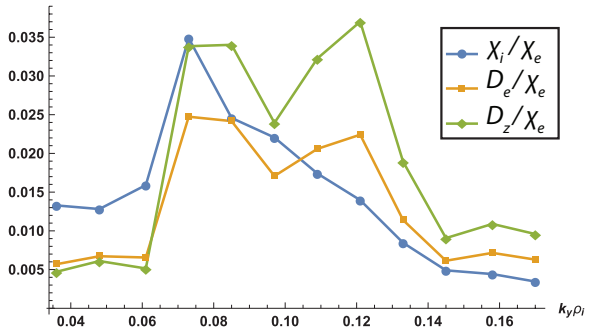

FIG. 8. Transport ratios of global linear simulations of the 174082 pedestal. These ratios are expected to be very small for both ETG and MTM instabilities[14].

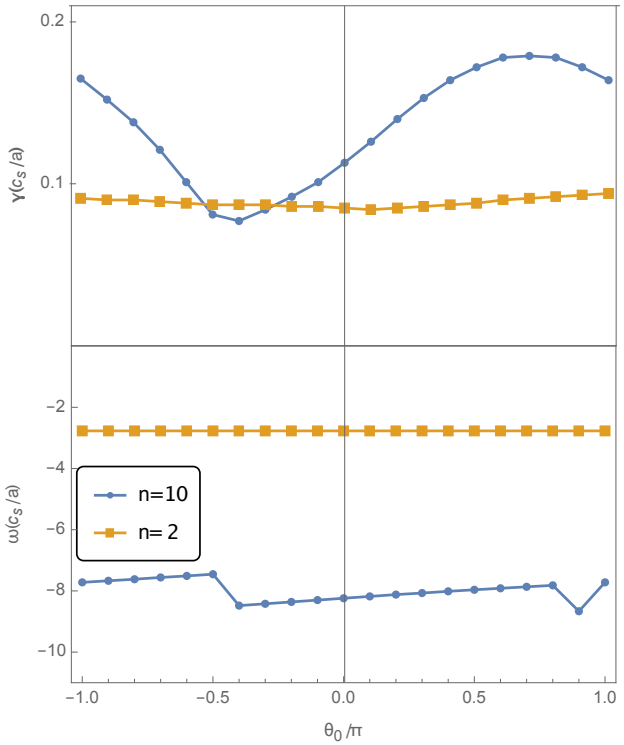

FIG. 9. Scan of ballooning angle for the $n = 2$ and $n = 10$ local linear instabilities. Change in growth rates for higher-n modes are expected, while the low-n slab-like modes remain unaffected.

and in closer proximity (in n) to the slab branch.

We first examine the ballooning-angle dependence of two modes representative of the two branches, which is shown in Fig. 9 (this can only be examined for local linear simulations). The low-n mode exhibits very weak θ_0 dependence in contrast with the strong dependence of the higher-n mode consistent with the characterization of each as slab or curvature-driven, respectively. The lower frequency electromagnetic fluctuation is associated with a lower toroidal mode number, due to the linear dependence of ω_{*e} on $k_y\rho_i$.

We also investigate the collisionality dependence of the modes. As shown in Fig. 10, the higher-n branch asymptotes to a constant, non-negligible, growth rate in the low collisionality limit while the lower-n branch transitions to an ion diamagnetic-directed instability as collisionality approaches zero, indicating that this low-n MTM is completely stabilized in this limit. Once again, this collisionality dependence is consistent with the modes' characterization as slab-like and curvature driven.

Several recent papers have investigated (analytically and numerically) collisionless microtearing instabilities[13,43,44].

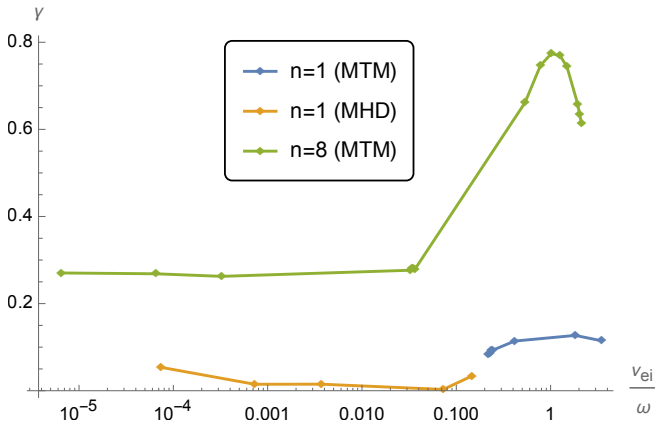

FIG. 10. Dependence of local microtearing growth rates as a function of electron-ion collisionality. For this scan: $\rho_{tor} = 0.96, k_y\rho_i = 0.15$ for the $n = 8$ simulation and $k_y\rho_i = 0.02$ for the $n = 1$ simulation. Non-monotonic dependence on collisionality is a key characteristic of MTM's[45], and is shown quite clearly for both $k_y\rho_i$'s.

C. NEO Results

While the anomalous transport in the edge region is of considerable interest, a significant portion of ion heat flux can be attributed to neoclassical transport. Using the code NEO[46,47], the neoclassical transport levels for ions, electrons, and impurities are calculated. Figure11 shows the total neoclassical heat loss from all three species, indicating that neoclassical transport is significant, particularly towards the pedestal top. Pedestal top ($\rho \approx 0.94$) neoclassical heat losses are significant and decrease in the steep gradient region. For reference, we expect a total of $4.67MW$ of power losses in the pedestal, so these transport levels are significant. Figure12 shows the total particle loss due to neoclassical transport. Although neoclassical transport is generally weak in the particle channel, these particle transport levels are close to those predicted by SOLPS modeling[12]: $\sim 10^{21}$ particles/s. In summary, these results suggest that neoclassical transport is important in the ion heat channel and in the particle channel.

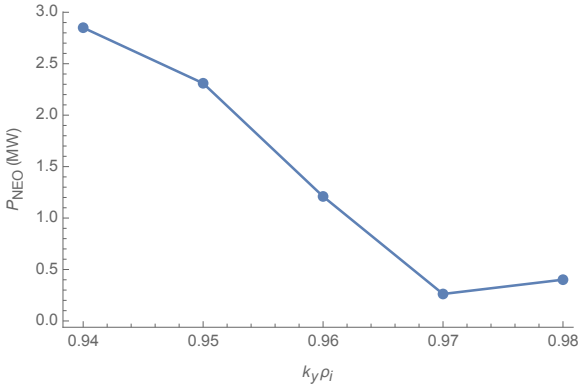

FIG. 11. Heat lost to neoclassical transport across the pedestal. Pedestal top losses are significant, but drop by mid-pedestal.

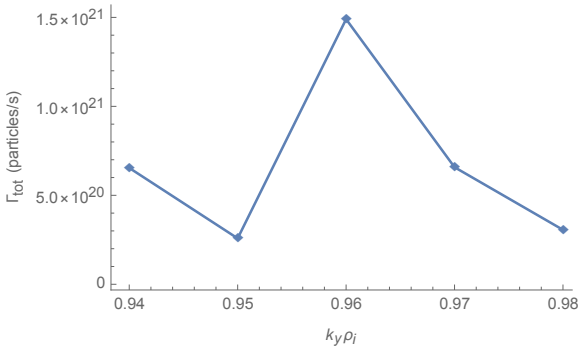

FIG. 12. Neoclassical particle losses across the pedestal. Values are consistent with the results of SOLPS calculations of particle flux.

D. Local Nonlinear Simulations

To obtain estimates of anomalous power losses, fluctuation amplitudes, and transport coefficients, nonlinear simulations are required. Simulations of local nonlinear ETGs are performed at multiple radial locations in the pedestal pedestals by setting $k_{y,min}\rho_i = 5$ and $k_{y,max} = 240$, with sensitivity tests in the gradient drive to ensure that variations in the equilibrium profiles do not result in major changes to transport coefficients at that location, increasing $\nabla T_e/T_e$ by 20% and decreasing $\nabla n_e/n_e$ by 20% to keep ∇P_e fixed. The nominal profiles resulted in insignificant electron heat flux ($P_{ETG} = 0.015$ MW at its highest) and the modified profiles gave much higher losses ($P_{ETG} = 1.26$ at its highest), but the resulting increase in energy loss is still not enough to account for the experimentally observed losses as shown in Figure 13.

Nonlinear simulations ($k_{y,min}\rho_i = 0.02 - 0.24$) of microtearing modes were carried out at the location of highest ∇T_e. The simulations extend from $k_y\rho_i = 0.02 - 0.94$ and employ kinetic electrons and adiabatic ions. The result is a high level of magnetic flutter ($Q_{em} = 1.14$ MW). An additional simulation with the same increase of $\nabla T_e/T_e$ by 20% and decrease of $\nabla n_e/n_e$ by 20% resulting in $Q_em = 1.32MW$. The snapshot of magnetic potential depicted in Figure 14 shows a contour plot of the fluctuations caused by the microtearing modes. The corresponding heat flux spectrum is shown in Figure 15.

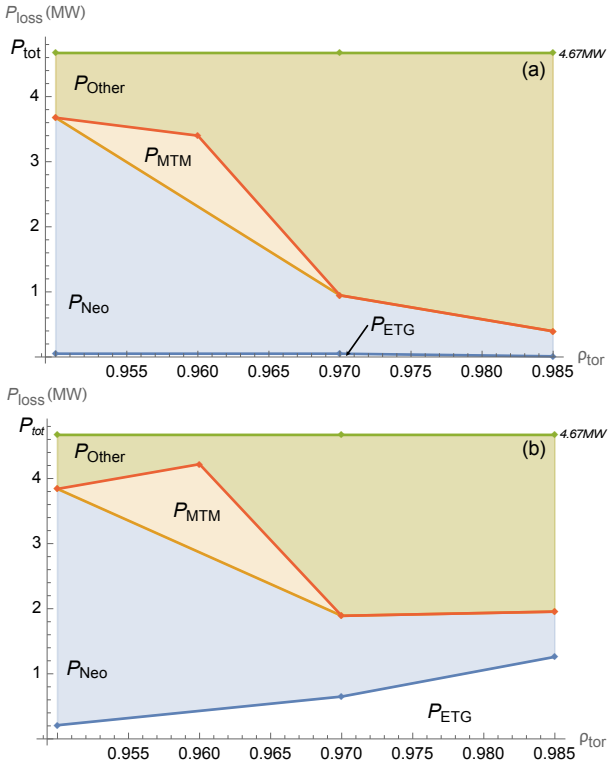

FIG. 13. Power losses at different radial locations across the pedestal, with no modification to the profile data (a). Power losses across the pedestal with modified temperature and density gradients (b). Note that the radial extent of the MTM transport may be broader than shown here since this is a local simulation.

Sensitivity studies of nonlinear microtearing saturation are currently underway, with variation of multiple driving mechanisms including β, ∇T_e, and ν_{ei} with the target of formulating reduced models for pedestal MTM transport.

E. Microtearing Diffusivity Model

In this section, we compare predicted electromagnetic transport levels with a simple model relating heat diffusivity as directly proportional to the fluctuation amplitude through a Rechester-Rosenbluth-like relation[48],

$$\chi_e^{em} = \chi_{e\|}\langle(\tilde{B}_x/B_{ref})^2\rangle, \tag{2}$$

where the parallel diffusivity is given by

$$\chi_{e\|} \approx \frac{1}{k_\|}\left(\frac{T_e}{m_e}\right)^{1/2} \tag{3}$$

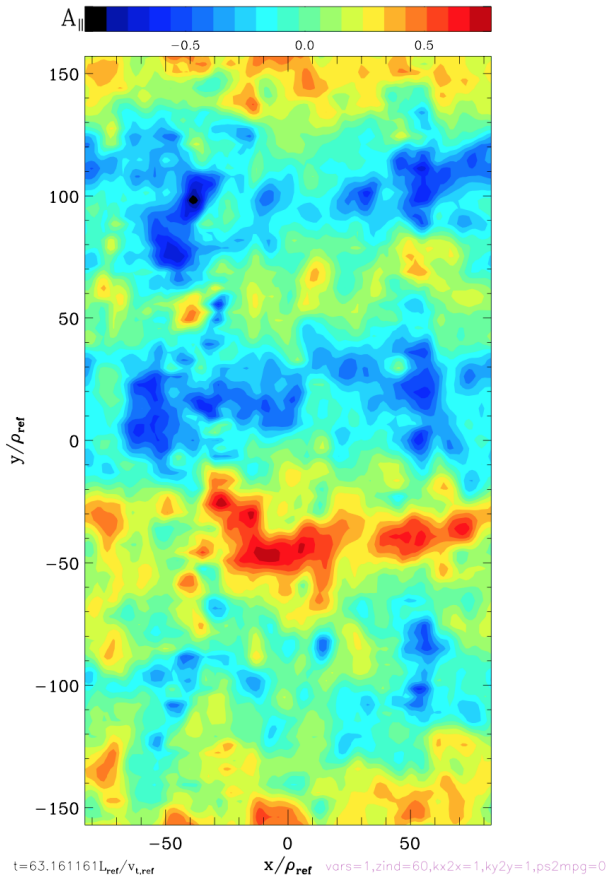

FIG. 14. Snapshot of $A_\parallel$ from a local nonlinear microtearing simulation. Strong electromagnetic heat flux is found at an experimentally relevant level, $Q_{em} = 1.14$ MW. Density fluctuations register at levels far below the predicted KBM threshold, $\delta n/n_0 = 0.01$ for this case. Electrostatic heat flux is far below the electromagnetic component, $Q_{es} = 0.05$ MW, offering further evidence that the observed turbulence is driven by microtearing modes.

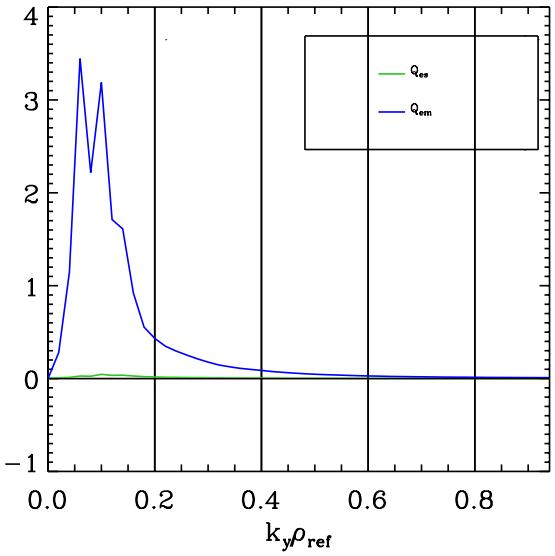

FIG. 15. Flux spectrum for a local nonlinear microtearing mode, in GyroBohm units $cp\rho^{*2}$. The electromagnetic component, Q_{em} (blue) is significantly higher than the electrostatic flux, Q_{es} (green).

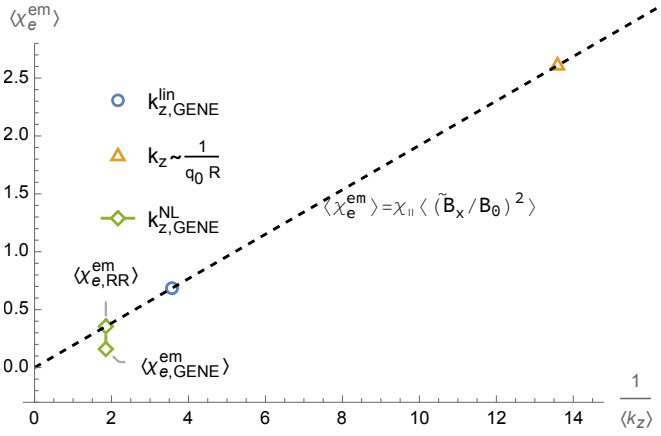

FIG. 16. Plot of electromagnetic electron heat diffusivity as a function of inverse parallel wavenumber. The bottom green diamond represents the k_z and heat diffusivity both calculated directly from a nonlinear GENE simulation, while the top green diamond shows the approximation made using the Rechester-Rosenbluth formula of Eq.2. Note that the nonlinear values are the same order of magnitude as the linear GENE result (blue circle), but differ by an order of magnitude from the q_0R approximation (gold triangle).

To test the validity of this model, we compare this estimate to the results found in GENE. In the nonlinear GENE simulation of this discharge, the electromagnetic electron heat diffusivity is found to be $\chi_e^{em} = 0.16m^2/s$, the $\tilde{B}_r/B_0 = 0.055$. The calculation using the $k_\parallel$ from the eigenmode at the peak linear growth rate and the magnetic fluctuation amplitude from the nonlinear simulation, gives $\chi_e^{em} = 0.68m^2/s$, which is reasonably close to the nonlinear simulation (i.e., a factor of ~ 4 is required to match). Using the Rechester-Rosenbluth formula to predict χ_e^{em} using k_z and $\tilde{B}_r/B_0$ both from the nonlinear simulation fares quite well, $\chi_e^{em} = 0.355365$ (a factor of ~ 2 discrepancy). Estimating the diffusivity using the standard approximation $1/k_\parallel = q_0R$ fares much more poorly: $\chi_e^{em} = 2.61m^2/s$. Fig. 16 compares these diffusivities and the method of $k_\parallel$ or $\chi_{e,\parallel}$ used in their calculation.

The parallel wavenumbers from GENE simulations are found to be much larger than the simplified $1/(q_0R)$ prediction, consistent with the slab-like nature of the low-k_y MTM. For each calculation, the magnetic fluctuation amplitude used is from the nonlinear GENE simulation.

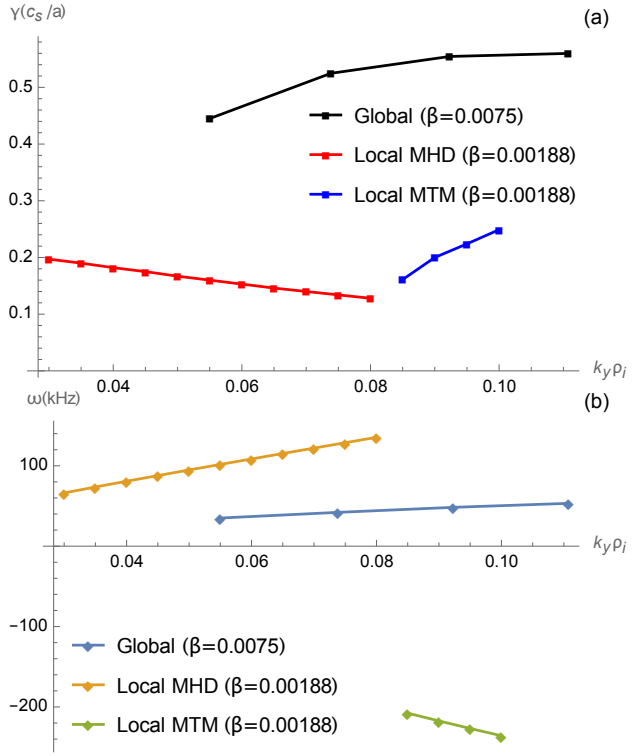

FIG. 17. Growth rates (a) and real frequencies (b) of global MHD modes (black, light blue), local MHD instabilities (red, gold), and local microtearing instabilities (dark blue, green) for modified β simulations. Local simulations find MHD modes as the fastest-growing mode at lower β than their global counterpart, but transition to unstable MTM's at a critical $k_r\rho_i$

F. Global and local scan of MHD-like modes

To probe the nature of possible subdominant, low-frequency MHD instabilities, we study modified scenarios that produce such modes. Unstable local MHD modes are quite easy to produce. However, global MHD modes are much more challenging to produce for this scenario.

These results are obtained by increasing the pedestal β to levels surpassing the nominal experimental value. By increasing the value of the pedestal beta by a factor of 2.4 for global and 1.8 for flux-tube simulations, keeping the profile gradients fixed, we identify unstable MHD modes. These values of β are clearly beyond experimental uncertainties. However, two considerations suggest that MHD modes may be unstable at more realistic values of β: (1) the mode is likely unstable at much lower values of β but it is subdominant to MTM, and (2) for global, the mode is likely more unstable with a more-realistic outer radial boundary condition, which is a Dirichlet boundary just inside the separatrix in our GENE simulations (MHD stability is well-known to depend sensitively on the vacuum region). Moreover, there are additional uncertainties in density and temperature gradients that we could probe.

For the lowest toroidal mode numbers, the resulting MHD-like instability becomes the most unstable mode. The real frequencies and growth rates for both local and global MHD-like simulations are shown in Figure 17. Figure 18 shows transport ratios for a set of high-β simulations, which are consistent with the expectations from Ref.[14]. Note that the global simulations include the Doppler shift, but the local simulations do not, which should be considered in the context of the mode frequencies shown in Fig. 17.

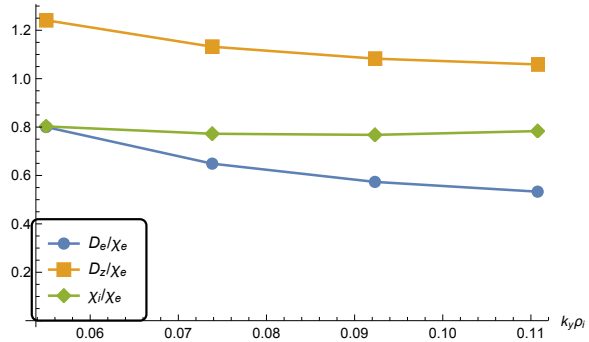

FIG. 18. Global simulations with $\beta = 0.0075$ at the simulation center have vastly different transport ratios than the baseline cases, with values that are consistent with the "fingerprints" of MHD-like modes.

The characteristics of these modes are consistent with expectations of MHD-like modes, namely significant particle diffusivity relative to heat diffusivity, real frequencies in the ion diamagnetic direction, similar heat transport in the ion and electron channels ($\chi_i/\chi_e \approx 1$), and heat transport dominated by electrostatic fluctuations ($Q_{em}/Q_{es} < 1$). The global instability appears to be an Alfvénic mode, as it satisfies the relation $\omega \approx k_\parallel v_A$. The parity appears to be ballooning, rather than tearing, as shown in Figure19. Further investigation into the nature of this instability is left for future work.

Another "fingerprint" that distinguishes microtearing instabilities from MHD-like modes comes in the form of parallel electric field cancellation. In kinetic MHD modes, $E_\parallel$ is near zero while microtearing modes have a finite electric field linked to Ohm's Law and the current that is driven around the rational surfaces. Figure 21 shows the normalized electric field cancellation factor as calculated by,

$$\hat{E}_\parallel = \frac{\int dz|-\partial_z\phi + i\omega A_\parallel|}{\int dz|\partial_z\phi| + \int dz|i\omega A_\parallel|}, \tag{4}$$

differs significantly between MTM and MHD instabilities.

We note that this $E_{||}$ criterion for MHD modes is stronger the closer the mode is to ideal MHD. Extended MHD codes such as NIMROD have the capacity to model considerable non-ideal behavior. Consequently, such MHD codes are clearly not constrained to model

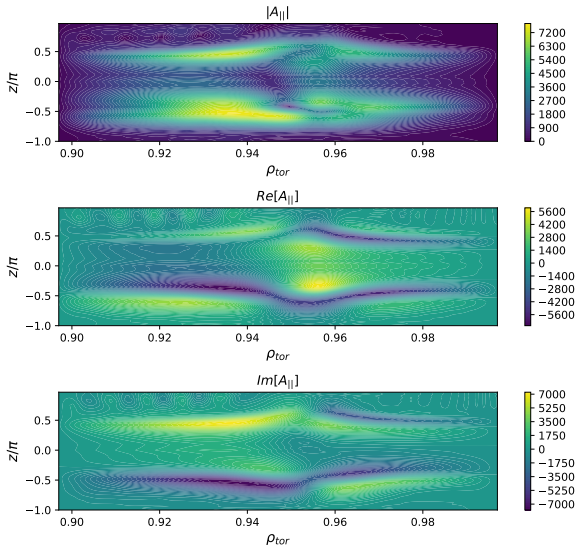

FIG. 19. Contour plot of $A_{||}$ for the MHD-like instability. The mode has odd parity, and is radially extended, with peak amplitude away from the midplane.

$E_{||} \sim 0$ modes and the MHD-like transport ratios that stem from this constraint[14].

IV. COMPARISON OF TRANSPORT AND FLUCTUATIONS FROM MTM AND MHD

In this section, we will compare MTMs with MHD modes with the goal of drawing conclusions about their respective roles in pedestal transport. To that end, we will examine the sets of gyrokinetic simulations described above: (1) global and local linear MTMs, (2) local nonlinear MTMs, and (3) global and local linear MHD modes. Each set of simulations has its inherent strengths and weaknesses. The global linear MTM simulations capture background profile variation, which has been shown to be important in the past, and include kinetic ions (allowing for particle flux information), but do not predict fluctuation levels. The local nonlinear MTM simulations neglect background profile variation and kinetic ions but do predict a nonlinear saturation amplitude and heat flux. Nonlinear MHD simulations using gyrokinetics are extremely challenging and so we limit the investigation to linear. The global linear MHD simulations include background profile variation and information regarding the width of the drive region[49], but extremely high β is required to produce an MHD mode. In contrast, the local linear MHD neglects the radially-nonlocal effects but does not require such extreme values of β to destabilize.

These simulations will be examined in the context of the following experimental (or edge modeling) data:

- Magnetic spectrograms.
- The ratio of density fluctuation amplitude to heat flux.
- The ratio of magnetic fluctuation amplitude to density fluctuation amplitude.
- The ratio of particle flux to heat flux (calculated from SOLPS simulations).

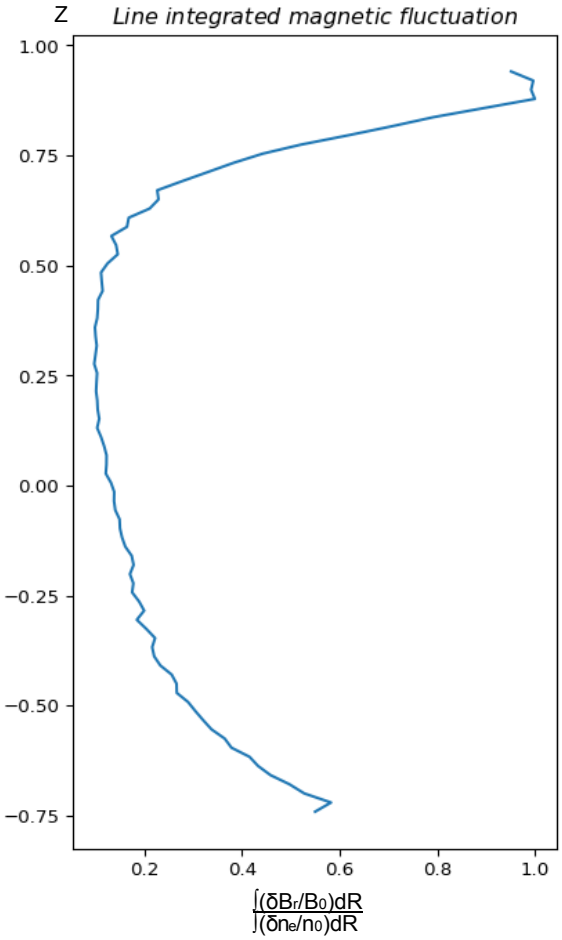

FIG. 20. Ratio of normalized line-integrated magnetic fluctuation to normalized density fluctuation calculated using from a representative GENE MTM simulation.

For some of these analyses, it is important to keep in mind that experimental diagnostics often target the outboard midplane. For instabilities such as the ITG (in the core) or KBM, this coincides with the peak fluctuation amplitude. However microtearing instabilities in the pedestal peak off-axis, leading to a minimum in fluctuations at the outboard midplane. Figure 20 depicts the ratio of line-averaged magnetic to density fluctuations as a function of height (above or below the outboard midplane). Consequently, although measures of outboard midplane fluctuations are highly useful, they are not able

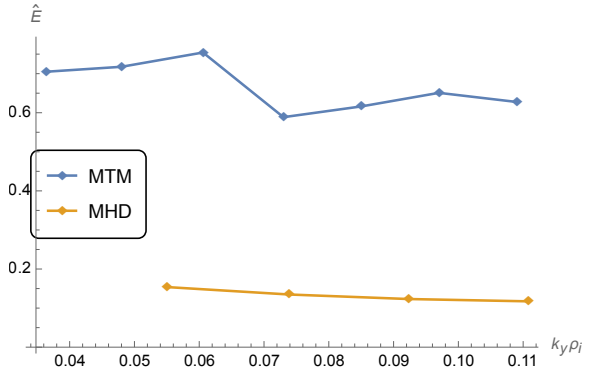

FIG. 21. Measure of $\hat{E}_{\|}$ for simulations with baseline (blue) and modified (gold) profiles. The MHD-like instabilities resulting from increased β have significant parallel electric field cancellation while the nominal microtearing cases have a finite parallel electric field, consistent with the predictions of theory[14].

to diagnose important aspects of our MTM predictions.

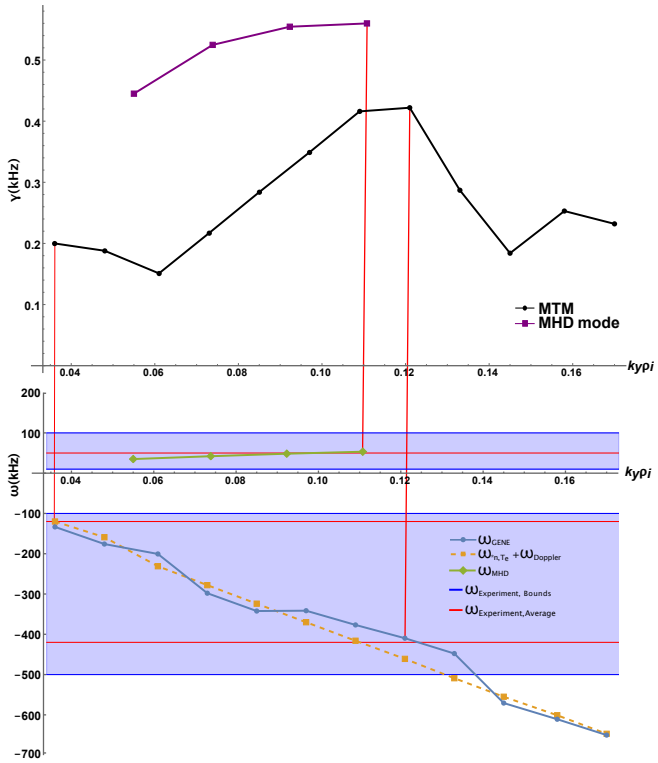

FIG. 22. Plot of growth rates (Top) and real frequencies (Bottom) for a spectrum of microtearing and MHD modes in shot 174082. The real frequencies obtained from GENE (blue circles) are compared to the analytic predictions (yellow squares) and experimentally observed (blue shaded region) values.

A. Magnetic Spectrograms

Figure 22 shows that the fastest-growing linear MTM is approximately at the same real frequency ($\sim 400kHz$) as the experimentally observed signal in Figure 1. The lower band in the spectrogram $f \sim 100-200kHz$ also is quite close to the frequency of the low k_y MTM peak (slightly over $100kHz$). The experimentally observed frequency range is the broadest at the time from which the equilibrium data was acquired ($t = 3000ms$), which is perhaps consistent with the unstable MTMs spanning the whole frequency range.

There is also a low frequency band in the spectrogram (circled in black in Fig. 1), which we will compare with the MHD frequencies. The mode frequencies of the (global, which accounts for the Doppler shift) simulated MHD instabilities range from $35-55kHz$ (recall Fig. 17), consistent with this band.

In summary, the higher frequency bands correspond quite well with the peaks in the global MTM growth rate spectrum, while the lower band corresponds quite well with the simulated MHD modes. We find it plausible that both are active simultaneously in the pedestal and affect different transport channels. The MTM instabilities would mediate the electron heat flux and temperature profiles, while the MHD modes would be limited primarily to particle transport[14]. We further explore the plausibility of this picture in the following sections.

B. Ratio of Magnetic Fluctuation Amplitude to Density Fluctuation Amplitude

The ratio of magnetic fluctuations to density fluctuations is also a quantity that could differ between modes, and can be measured by the recently developed Faraday Effect Radial Interferometer Polarimeter diagnostic (RIP)[10,11] (although such fluctuation measurements are not available for this discharge).

MHD-like modes are expected to exhibit higher relative density fluctuation amplitudes in comparison with MTM modes. However, simulations of the increased β equilibria show that the MHD-like modes exhibit a $\frac{\delta\bar{B}/B}{\delta\bar{n}/n}$ ratio that is similar to (and, in fact, generally larger than) the microtearing counterpart, as shown in Figure 23. Consequently, this metric can not cleanly discriminate between the two modes at least for this study.

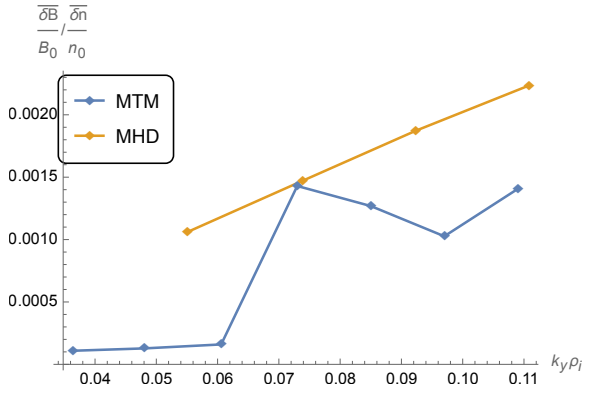

FIG. 23. The ratio of $\frac{\delta \bar{B}/B}{\delta \bar{n}/n}$ is calculated for simulations of both the baseline equilibrium profiles and profiles with modified β_e with the integration taking place across the midplane.

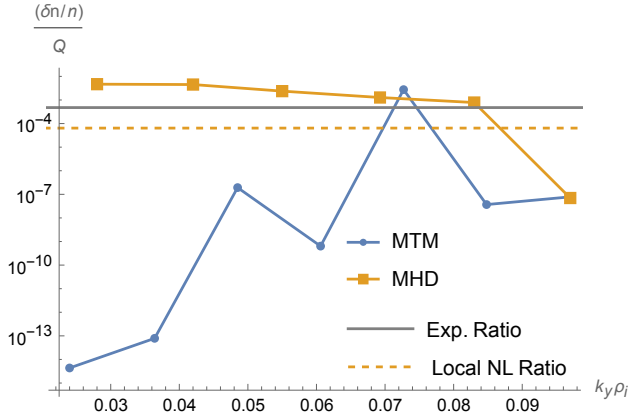

FIG. 24. Ratio of $(\delta n/n_0)/Q$ for both microtearing and MHD-like global simulations. The solid grey line is the experimental estimate calculated using the noise floor of the BES diagnostic ($\delta n/n_0 = 0.001$) and an estimate of anomalous power lost in this discharge ($Q = 2.1MW$). The dashed yellow line is the ratio from a local nonlinear simulation of shot 174082, ($\delta n/n_0 = 0.0000732478$, $Q = 1.14MW$).

C. Ratio of Density Fluctuation Amplitude to Heat Flux

Here we examine another prospective experimentally-accessible metric, the ratio of density fluctuations to heat flux $(\delta n/n_0)/Q$. In this discharge, Beam Emission Spectroscopy (BES) is used to place an upper bound on the possible density fluctuation level. Shot 174082 is distinctive because the density fluctuation amplitude falls below the noise level of BES measurements. This places an upper bound on the possible fluctuation levels ($\delta n/n \approx 0.1\%$), which we will use in comparison with simulated fluctuation amplitudes.

Fig. 24 shows this ratio for the MTM and MHD simulations, as well as for the threshold experimental fluctuation level $\delta_n/n \approx 0.1$ described above. As shown in Fig. 24, the nonlinear MTM simulation produces a ratio quite close to this experimental estimate. However, the estimate from linear MHD is somewhat larger. Since this density fluctuation level is an upper bound, this would imply that the MHD mode is unlikely to account for the bulk of the heat flux. This does not eliminate the possibility of MHD fluctuations since (1) the value of $(\delta n/n_0)/Q$ for the MHD modes is not too much larger than the experimental upper bound, and (2) even at a low fluctuation level, the MHD modes could still strongly impact the particle transport channel.

In summary, this analysis is consistent with the nonlinear MTM simulations described above, but cannot rule out the possibility of MHD fluctuations as well. The combined MTM and MHD scenario proposed above remains a possibility.

D. Ratio of Particle Flux to Heat Flux

As a final comparison between MHD and MTM, we compare the ratio of particle to heat flux. A robust feature of MHD modes is that they produce roughly equal diffusivity in the particle and heat channels: $D \sim \chi$ (this criterion is increasingly stringent with proximity to the ideal MHD limit). In contrast, MTMs produce much higher heat transport: $D/\chi \ll 1$. The particle diffusivity is difficult to diagnose experimentally, but edge modeling can provide an estimate. SOLPS was used to this end for this discharge as described in[12].

Figure 25 depicts the values of Γ_{tot}/Q_{tot} for the linear simulations of MTMs (global) and MHD-like modes (global and local) along with the SOLPS prediction (recall that the nonlinear MTM simulations cannot be used here because of the adiabatic ion approximation). The unstable microtearing modes agree with the value found in SOLPS, whereas the MHD modes are higher than the SOLPS prediction. Local values of Γ_{tot}/Q_{tot} in kinetic MHD modes are comparable to their global counterparts. This implies that if the MHD modes are active, their impact would be largely limited to the particle channel. Our conclusion from this analysis is similar to that of the last subsection: MHD modes may be active but only at a level that can impact the particle transport rather than the heat transport.

V. SUMMARY OF RESULTS

Global GENE simulations of DIII-D shot 174082 have shown that the most unstable mode for a series of toroidal wavenumbers, with real frequencies corresponding to a broad band of observed magnetic fluctuations, is a microtearing mode. Simulations also indicate that ETG turbulence and neoclassical effects cannot account for the total heat transport observed in this shot. A significant cause of energy loss in the pedestal is found to be the microtearing mode, as evidenced by a combination of non-

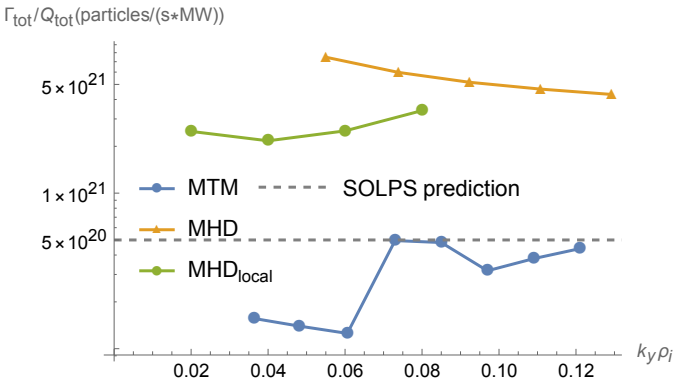

FIG. 25. Ratio of total surface-averaged particle flux, Γ, to total heat flux, Q, in gyroBohm units for each respective quantity. Particle fluxes are predicted to be higher for MHD-like instabilities than MTM's. This is confirmed for global GENE simulations of these instabilities, as the MHD ratio of Γ_{tot}/Q_{tot} is an order of magnitude higher than the MTM ratio.

linear local, linear local, and linear global simulations of the pedestal region. The MTM is the fastest-growing linear instability, with gyrokinetic "fingerprints" that correspond well with the expectations of analytic theory, the observations of experimental diagnostics, and the results gyrokinetic simulations of carefully reconstructed equilibria. Notably, the MTM frequencies are in good agreement with bands in the magnetic spectrogram.

Modifying the equilibrium past the kinetic MHD β limit shows that an unidentified MHD mode, possibly a toroidal Alfvén eigenmode, becomes unstable, with fluctuation frequencies consistent with a band of fluctuations observed in the experimental magnetic spectrogram. This low-frequency mode may be responsible for inter-ELM particle transport. Further characterization of this instability is left for a future project.

VI. CONCLUSIONS

This paper has investigated transport and magnetic fluctuations in the pedestal using gyrokinetic (using the GENE code) simulations for DIIID discharge 174082. The main findings are as follows. Simulated MTM frequencies are in good agreement with corresponding frequency bands in the magnetic spectrogram and nonlinear MTM produce experimentally-relevant transport levels. We conclude that it is very likely that MTMs are responsible for the observed magnetic fluctuations and that it is likely that they also limit the electron temperature pedestal. We also speculate that MHD modes are responsible for low frequency fluctuations found in the magnetic spectrogram. Although GENE does not identify unstable MHD modes for the nominal equilibrium reconstruction, high beta simulations produce MHD modes with frequencies in the right range.

We investigate several metrics that may inform or constrain the possible roles of MHD and MTMs. Two metrics are, perhaps surprisingly, ineffective at discriminating between the two classes of fluctuations. The ratio of density fluctuation amplitudes to magnetic fluctuation amplitudes is comparable for MHD and MTM based on linear GENE simulations. Likewise, the ratio of density fluctuation amplitudes to heat flux is somewhat larger for MHD modes, but not so large as to preclude their activity in this discharge. One metric, however, clearly distinguishes between MHD and MTM: the ratio of particle to heat diffusivity is much smaller for MTMs in agreement with SOLPS predictions. While this does not preclude the possible activity of MHD modes, it does limit their role to the particle transport channel.

We also investigate neoclassical and ETG as prospective transport mechanisms. Neoclassical transport (as calculated with NEO) produces substantial ion heat flux and particle flux roughly in agreement with SOLPS predictions. ETG transport is negligible for the nominal gradients. For simulations with moderately higher eta (within experimental uncertainties), ETG transport becomes relevant although still somewhat below experimental expectations.

Two possible transport pictures emerge, (1) one without MHD fluctuations and (2) one including MHD fluctuations. In scenario (1) (negligible MHD fluctuations), neoclassical transport accounts for the particle channel and ion heat channel while ETG and MTM supply the electron heat transport. Simulated values for these (neoclassical, ETG, MTM) transport mechanisms are consistent with this picture. In scenario (2), MHD combines with neoclassical to account for the particle transport and other channels are the same as in scenario one. Although we are unable to probe this possibility with nonlinear MHD simulations, there is a low frequency fluctuation band in the spectrogram that may signal such MHD activity.

VII. ACKNOWLEDGEMENTS

This work is funded by US DOE under DE-FC02-04ER54698. A portion of this study's data analysis was performed using the OMFIT integrated modeling framework[50]. This manuscript has been authored by UT-Battelle, LLC, under contract DE-AC05-00OR22725 with the US Department of Energy (DOE). The publisher acknowledges the US government license to provide public access under the DOE Public Access Plan (http://energy.gov/downloads/doe-public-access-plan).

[1] Fritz Wagner, G Fussmann, T Grave, M Keilhacker, M Kornherr, K Lackner, K McCormick, ER Müller, A Stäbler, G Becker, et al. Development of an edge transport barrier at the h-mode transition of asdex. *Physical Review Letters*, 53(15):1453, 1984.

[2] D.R. Hatch, M.T. Kotschenreuther, S. Mahajan, P. Valanju, F. Jenko, D. Told, T. Görler, and S. Saarelma. Microtearing turbulence limiting the JET-ILW pedestal. *Nuclear Fusion*, 56(10):104003, 2016.

[3] K. Stimmel, A. Bañón Navarro, T. Happel, D. Told, T. Görler, E. Wolfrum, J. P. Martin Collar, R. Fischer, P. A. Schneider, and F. Jenko. Gyrokinetic investigation of the asdex upgrade i-mode pedestal. *Physics of Plasmas*, 26(12):122504, 2019.

[4] J. Chowdury, Y. Chen, W. Wan, S.E. Parker, W. Guttenfelder, and J.M. Canik. Particle-in-cell δf gyrokinetic simulations of the microtearing mode. *Physics of Plasmas*, 23(1):012513, 2015.

[5] D.R. Hatch, M.T. Kotschenreuther, S.M. Mahajan, M.J. Pueschel, C. Michoski, G. Merlo, E. Hassan, A.R. Field, L. Frassinetti, C. Giroud, et al. Microtearing modes as the source of magnetic fluctuations in the jet pedestal. *Nuclear Fusion*, 61(3):036015, 2021.

[6] Arash Ashourvan, R. Nazikian, E. Belli, J. Candy, D. Eldon, B. A. Grierson, W. Guttenfelder, S. R. Haskey, C. Lasnier, G. R. McKee, and C. C. Petty. Formation of a high pressure staircase pedestal with suppressed edge localized modes in the diii-d tokamak. *Phys. Rev. Lett.*, 123:115001, Sep 2019.

[7] W Guttenfelder, J Candy, SM Kaye, WM Nevins, E Wang, RE Bell, GW Hammett, BP LeBlanc, DR Mikkelsen, and H Yuh. Electromagnetic transport from microtearing mode turbulence. *Physical review letters*, 106(15):155004, 2011.

[8] F.M. Laggner, E. Wolfrum, M. Cavedon, F. Mink, E. Viezzer, M.G. Dunne, P. Manz, H. Doerk, G. Birkenmeier, R. Fischer, et al. High frequency magnetic fluctuations correlated with the inter-elm pedestal evolution in asdex upgrade. *Plasma Physics and Controlled Fusion*, 58(6):065005, 2016.

[9] A. Diallo, R.J. Groebner, T.L. Rhodes, D.J. Battaglia, D.R. Smith, T.H. Osborne, J.M. Canik, W. Guttenfelder, and P.B. Snyder. Correlations between quasi-coherent fluctuations and the pedestal evolution during the inter-edge localized modes phase on diii-d. *Physics of Plasmas*, 22(5):056111, 2015.

[10] J. Chen, D.L. Brower, W.X. Ding, Z. Yan, T. Osborne, E. Strait, M. Curie, D.R. Hatch, M.T. Kotschenreuther, X. Jian, et al. Internal measurement of magnetic turbulence in elmy h-mode tokamak plasmas. *Physics of Plasmas*, 27(12):120701, 2020.

[11] J. Chen, D.L. Brower, W.X. Ding, Z. Yan, M. Curie, M.T. Kotschenreuther, T. Osborne, E. Strait, D.R. Hatch, M.R. Halfmoon, and et al. Pedestal magnetic turbulence measurements in elmy h-mode diii-d plasmas by faraday-effect polarimetry. *Physics of Plasmas*, 28(2):022506, 2021.

[12] D.R. Hatch, M.T. Kotschenreuther, S.M. Mahajan, M.R. Halfmoon, E. Hassan, G. Merlo, C. Michoski, J. Canik, A.C. Sontag, and I. Joseph. Final report for the fy19 fes theory performance target. 10 2019.

[13] Ehab Hassan, D.R. Hatch, M.R. Halfmoon, M. Curie, M.T. Kotchenreuther, S.M. Mahajan, G. Merlo, R.J. Groebner, A.O. Nelson, and A. Diallo. Identifying the microtearing modes in the pedestal of DIII-d h-modes using gyrokinetic simulations. *Nuclear Fusion*, 62(2):026008, dec 2021.

[14] M. Kotschenreuther, X. Liu, D. R. Hatch, S. Mahajan, L. Zheng, A. Diallo, R. Groebner, J.C. Hillesheim, C.F. Maggi, C. Giroud, et al. Gyrokinetic analysis and simulation of pedestals, to identify the culprits for energy losses using fingerprints. *Nuclear Fusion*, 59(9):096001, 2019.

[15] M. Curie, M.R. Halfmoon, J. Chen, D.R. Hatch, D.L. Brower, E. Hassan, M.T. Kotschenreuther, M.J. Mahajan, and R.J. Groebner. Gyrokinetic simulations compared with magnetic fluctuations diagnosed with a faraday-effect radial interferometer-polarimeter in the diii-d pedestal.

[16] A.O. Nelson, F.M. Laggner, A. Diallo, D. Smith, A. Xing, R. Shousha, and E. Kolemen. Time-dependent experimental identification of inter-elm microtearing modes in the tokamak edge on diii-d. *Nuclear Fusion*, 61:116038, 2021.

[17] DJ Applegate, CM Roach, JW Connor, SC Cowley, W Dorland, RJ Hastie, and N Joiner. Micro-tearing modes in the mega ampere spherical tokamak. *Plasma Physics and Controlled Fusion*, 49(8):1113, 2007.

[18] H. Doerk, F. Jenko, M.J. Pueschel, and D.R. Hatch. Gyrokinetic microtearing turbulence. *Physical Review Letters*, 106(15):15503, 2011.

[19] D.R. Hatch, M.J. Pueschel, F. Jenko, W.M. Nevins, P.W. Terry, and H. Doerk. Origin of magnetic stochasticity and transport in plasma microturbulence. *Physical Review Letters*, 108(5):235002, 2012.

[20] D.R. Hatch, M.T. Kotschenreuther, S. Mahajan, P. Valanju, and X. Liu. A gyrokinetic perspective on the JET-ILW pedestal. *Nuclear Fusion*, 57(17):036020, 2017.

[21] P.B. Snyder, R.J. Groebner, A.W. Leonard, T.H. Osborne, and H.R. Wilson. Development and validation of a predictive model for the pedestal height. 16:056118, 2009.

[22] F. Jenko, W. Dorland, M. Kotschenreuther, and B. N. Rogers. Electron temperature gradient driven turbulence. *Physics of Plasmas*, 7(5):1904–1910, 2000.

[23] Tobias Goerler, Xavier Lapillonne, Stephan Brunner, Tilman Dannert, Frank Jenko, Florian Merz, and Daniel Told. The global version of the gyrokinetic turbulence code gene. *Journal of Computational Physics*, 230(18):7053–7071, 2011.

[24] Z.A. Xing, D. Eldon, A.O. Nelson, M.A. Roelofs, W.J. Eggert, O. Izacard, A.S. Glasser, N.C. Logan, O. Meneghini, S.P. Smith, R. Nazikian, and E. Kolemen. Cake: Consistent automatic kinetic equilibrium reconstruction. *Fusion Engineering and Design*, 163:112163, 2021.

[25] A.O. Nelson, F.M. Laggner, R. Groebner, B.A. Grierson, O. Izacard, D. Eldon, M.W. Shafer, A. Leonard, D. Shiraki, A.C. Sontag, and et al. Setting the h-mode pedestal structure: variations of particle source location using gas puff and pellet fueling. *Nuclear Fusion*, 60(4):046003,

2020.

[26] A.M. Dimits, G. Bateman, M.A. Beer, B.I. Cohen, W. Dorland, G.W. Hammett, C. Kim, J.E. Kinsey, M.T. Kotschenreuther, A.H. Kritz, and et al. Comparisons and physics basis of tokamak transport models and turbulence simulations. *Physics of Plasmas*, 7(3):969–983, 2000.

[27] D.R. Hatch, M.J. Pueschel, F. Jenko, F.W. Nevins, P.W. Terry, and H. Doerk. Magnetic stochasticity and transport due to nonlinearly excited subdominant microtearing modes. *Physics of Plasmas*, 20(1):012307, 2013.

[28] A.B. Navarro, T. Happel, T. Görler, F. Jenko, J. Abiteboul, A. Bustos, H. Doerk, D. Told, and ASDEX Upgrade Team. Gyrokinetic studies of core turbulence features in asdex upgrade h-mode plasmas. *Physics of Plasmas*, 22(4):042513, 2015.

[29] X. Garbet, Y. Idomura, L. Villard, and T.H. Watanabe. Gyrokinetic simulations of turbulent transport. *Nuclear Fusion*, 50(4):043002, 2010.

[30] M.R. Fahey and J. Candy. Gyro: A 5-d gyrokinetic-maxwell solver. In *SC'04: Proceedings of the 2004 ACM/IEEE Conference on Supercomputing*, pages 26–26. IEEE, 2004.

[31] J. Chowdhury, S.H. Ku, J. Dominski, R. Hager, D. Mikkelsen, W. Guttenfelder, P. Porazik, and C.S. Chang. Gyrokinetic study of electron transport in nstx using xgc. In *APS Division of Plasma Physics Meeting Abstracts*, volume 2017, pages PP11–051, 2017.

[32] Nathan Howard, Chris Holland, Anne White, Matt Reinke, Terry Rhodes, Martin Greenwald, Jeff Candy, Alcator C-Mod Team, et al. The effect of itg/tem mix on gyrokinetic modeling of an alcator c-mod current scan. In *APS Division of Plasma Physics Meeting Abstracts*, volume 2013, pages CO4–006, 2013.

[33] Christopher Holland, Timothy C Luce, Brian A Grierson, Sterling P Smith, Alessandro Marinoni, Keith H Burrell, CC Petty, and EM Bass. Examination of stiff ion temperature gradient mode physics in simulations of diii-d h-mode transport. *Nuclear Fusion*, 61(6):066033, 2021.

[34] AE White, L Schmitz, GR McKee, C Holland, WA Peebles, TA Carter, MW Shafer, ME Austin, KH Burrell, J Candy, et al. Measurements of core electron temperature and density fluctuations in diii-d and comparison to nonlinear gyrokinetic simulations. *Physics of Plasmas*, 15(5):056116, 2008.

[35] D. R. Ernst, K. H. Burrell, W. Guttenfelder, T. L. Rhodes, A. M. Dimits, R. Bravenec, B. A. Grierson, C. Holland, J. Lohr, A. Marinoni, G. R. McKee, C. C. Petty, J. C. Rost, L. Schmitz, G. Wang, S. Zemedkun, and L. Zeng. Role of density gradient driven trapped electron mode turbulence in the h-mode inner core with electron heating. *Physics of Plasmas*, 23(5):056112, 2016.

[36] DR Hatch, M Kotschenreuther, SM Mahajan, G Merlo, AR Field, C Giroud, JC Hillesheim, CF Maggi, C Perez von Thun, CM Roach, et al. Direct gyrokinetic comparison of pedestal transport in jet with carbon and iter-like walls. *Nuclear Fusion*, 59(8):086056, 2019.

[37] R M Churchill, C S Chang, S Ku, and J Dominski. Pedestal and edge electrostatic turbulence characteristics from an XGC1 gyrokinetic simulation. *Plasma Physics and Controlled Fusion*, 59(10):105014, aug 2017.

[38] X. Liu. *Gyrokinetic simulation of pedestal turbulence using GENE*. PhD thesis, University of Texas at Austin, 2018.

[39] D. Jarema, H.J. Bungartz, T. Görler, F. Jenko, T. Neckel, and D. Told. Block-structured grids for eulerian gyrokinetic simulations. *Computer Physics Communications*, 198:105–117, 2016.

[40] D. Jarema, H.J. Bungartz, T. Görler, F. Jenko, T. Neckel, and D. Told. Block-structured grids in full velocity space for eulerian gyrokinetic simulations. *Computer Physics Communications*, 215:49–62, 2017.

[41] JL Larakers, Max Curie, DR Hatch, RD Hazeltine, and SM Mahajan. Global theory of microtearing modes in the tokamak pedestal. *Physical Review Letters*, 126(22):225001, 2021.

[42] Max Curie and JET DIII-D. Reduced predictive models for micro-tearing modes in the pedestal. In *APS Division of Plasma Physics Meeting Abstracts*, volume 2021, pages UI01–002, 2021.

[43] I Predebon and F Sattin. On the linear stability of collisionless microtearing modes. *Physics of Plasmas*, 20(4):040701, 2013.

[44] M. Hamed, M. Muraglia, Y. Camenen, and X. Garbet. Stability of a slab collisional microtearing mode. *Contributions to Plasma Physics*, 58(6-8):529–533, 2018.

[45] L.F. Drake and Y.C. Lee. Kinetic theory of tearing instabilities. *The Physics of Fluids*, 20(8):1341–1353, 1977.

[46] E A Belli and J Candy. Kinetic calculation of neoclassical transport including self-consistent electron and impurity dynamics. *Plasma Physics and Controlled Fusion*, 50(9):095010, jul 2008.

[47] EA Belli and J Candy. Full linearized fokker–planck collisions in neoclassical transport simulations. *Plasma physics and controlled fusion*, 54(1):015015, 2011.

[48] Moritz J Pueschel, M Kammerer, and F Jenko. Gyrokinetic turbulence simulations at high plasma beta. *Physics of Plasmas*, 15(10):102310, 2008.

[49] GW Hammett, W Dorland, and FW Perkins. Fluid models of phase mixing, landau damping, and nonlinear gyrokinetic dynamics. *Physics of Fluids B: Plasma Physics*, 4(7):2052–2061, 1992.

[50] O. Meneghini, S.P. Smith, L.L. Lao, O. Izacard, Q. Ren, J.M. Park, J. Candy, Z. Wang, C.J. Luna, V.A. Izzo, B.A. Grierson, P.B. Snyder, C. Holland, J. Penna, G. Lu, P. Raum, A. McCubbin, D.M. Orlov, E.A. Belli, N.M. Ferraro, R. Prater, T.H. Osborne, A.D. Turnbull, and G.M. Staebler. Integrated modeling applications for tokamak experiments with OMFIT. *Nuclear Fusion*, 55(8):083008, 2015.

[51] N.T. Gladd, J.F. Drake, C.L. Chang, and C.S. Liu. Electron temperature gradient driven microtearing mode. *The Physics of Fluids*, 23(6):1182–1192, 1980.

[52] R.D. Hazeltine, D. Dobrott, and T.S. Wang. Kinetic theory of tearing instability. *The Physics of Fluids*, 18(12):1778–1786, 1975.

[53] J.F. Drake, N.T. Gladd, C.S. Liu, and C.L. Chang. Microtearing modes and anomalous transport in tokamaks. *Physical Review Letters*, 44(15):994–997, 1980.

[54] B.A. Carreras, L. Garcia, and P.H. Diamond. Theory of resistive pressure-gradient-driven turbulence. *The Physics of Fluids*, 30(5):1388–1400, 1987.

[55] K. Itoh, S.I. Itoh, and A. Fukuyama. Theory of anomalous transport in high-aspect-ratio toroidal helical plasmas. *Physical Review Letters*, 69(7):1050–1053, 1992.

[56] S. Moradi, I. Pusztai, W. Guttenfelder, T. Fülöp, and Mollén. Microtearing modes in spherical and conventional tokamaks. *Nuclear Fusion*, 53(6):063025, 2013.

[57] D. Dickinson, C.M. Roach, S. Saarelma, R. Scannell, A. Kirk, and H.R. Wilson. Microtearing modes at the top of the pedestal. *Plasma Physics and Controlled Fusion*, 55(7):074006, 2013.

[58] T. Rafiq, J. Weiland, A.H. Kritz, L. Luo, and A.Y. Pankin. Microtearing modes in tokamak discharges. *Physics of Plasmas*, 23(6):062507, 2016.

[59] T. Rafiq, A.H. Kritz, J. Weiland, L. Luo, and E. Schuster. Study of the parametric dependence of linear and nonlinear microtearing modes in conventional tokamak discharges. *Physics of Plasmas*, 25(1):012504, 2017.

[60] F.W. Perkins and J.H. Doles III. Velocity shear and the $E \times B$ instability. *Journal of Geophysical Research (1896-1977)*, 80(1):211–214, 1975.

[61] P. Beyer, S. Benkadda, G. Fuhr-Chaudier, X. Garbet, P.H. Ghendrih, and Y. Sarazin. Nonlinear dynamics of transport barrier relaxations in tokamak edge plasmas. *Phys. Rev. Lett.*, 94:105001, Mar 2005.

[62] C.F. Figarella, S. Benkadda, P. Beyer, X. Garbet, and I. Voitsekhovitch. Transport reduction by rotation shear in tokamak-edge turbulence. *Phys. Rev. Lett.*, 90:015002, Jan 2003.

[63] A. Diallo, R.J. Groebner, T.L. Rhodes, D.J. Battaglia, D.R. Smith, T.H. Osborne, J.M. Canik, W. Guttenfelder, and P.B. Snyder. Correlations between quasi-coherent fluctuations and the pedestal evolution during the inter-edge localized modes phase on DIII-D. *Physics of Plasmas*, 22(5):056111, 2015.

[64] U Stroth. A comparative study of transport in stellarators and tokamakes. *Plasma Physics and Controlled Fusion*, 9(40):9–74, 1998.

[65] Radu Balescu. *Aspects of anomalous transport in plasmas*. CRC Press, 2005.

[66] R. Klages, G. Radons, and I.M. Sokolov. *Anomalous transport: foundations and applications*. John Wiley & Sons, 2008.

[67] F. Merz. *Gyrokinetic simulation of multimode plasma turbulence*. PhD thesis, Universität Münster, 2008.

[68] T. Xie, M.J. Pueschel, and D.R. Hatch. Quasilinear modeling of heat flux from microtearing turbulence. *Physics of Plasmas*, 27(8):082306, 2020.

[69] P.B. Snyder, T.H. Osborne, K.H. Burrell, R.J. Groebner, A.W. Leonard, R. Nazikian, D.M. Orlov, O. Schmitz, M.R. Wade, and H.R. Wilson. The eped pedestal model and edge localized mode-suppressed regimes: Studies of quiescent h-mode and development of a model for edge localized mode suppression via resonant magnetic perturbations. *Physics of plasmas*, 19(5):056115, 2012.

[70] D. Dickinson, C.M. Roach, S. Saarelma, R. Scannell, A. Kirk, and H.R. Wilson. Kinetic instabilities that limit β in the edge of a tokamak plasma: a picture of an h-mode pedestal. *Physical Review Letters*, 108(13):135002, 2012.

[71] CH Ma and XQ Xu. Global kinetic ballooning mode simulations in bout++. *Nuclear Fusion*, 57(1):016002, 2016.

[72] Arash Ashourvan, BA Grierson, DJ Battaglia, SR Haskey, and Timothy Stoltzfus-Dueck. Validation of the kinetic-turbulent-neoclassical theory for edge intrinsic rotation in diii-d. *Physics of Plasmas*, 25(5):056114, 2018.

[73] Frank Jenko, W Dorland, M Kotschenreuther, and BN Rogers. Electron temperature gradient driven turbulence. *Physics of plasmas*, 7(5):1904–1910, 2000.

[74] Tobias Goerler, Xavier Lapillonne, Stephan Brunner, Tilman Dannert, Frank Jenko, Florian Merz, and Daniel Told. The global version of the gyrokinetic turbulence code gene. *Journal of Computational Physics*, 230(18):7053–7071, 2011.

[75] Jacob R King, SE Kruger, KH Burrell, X Chen, AM Garofalo, RJ Groebner, KEJ Olofsson, AY Pankin, and PB Snyder. Mhd modeling of a diii-d low-torque qh-mode discharge and comparison to observations. *Physics of Plasmas*, 24(5):055902, 2017.